Chapter 6
Fatigue Properties

6.1 Introduction

In the present chapter, fatigue properties of materials are described in terms of the fatigue limit, fatigue curves (S-N curves) and a fatigue diagram. The properties are restricted to results of constant-amplitude (CA) tests on unnotched specimens ($K_t = 1.0$) It is generally thought that the results of these tests reflect the basic fatigue behavior of a material. Mechanical properties of a material should include fatigue properties, but quite often reporting of fatigue properties is restricted to the fatigue limit on unnotched specimens obtained in rotating beam experiments ($S_m = 0$).

If fatigue has to be considered as part of the design analysis of a structure, it is well recognized that a stress cycle is characterized by a stress amplitude (S_a) and a mean stress (S_m), see Figure 6.1. Instead of S_a and S_m, a second equivalent definition is given by $S_{\max}$ and $S_{\min}$, while a third one uses the stress range ΔS ($= 2S_a$) together with the stress ratio R, defined as

$$R = \frac{S_{\min}}{S_{\max}} \tag{6.1}$$

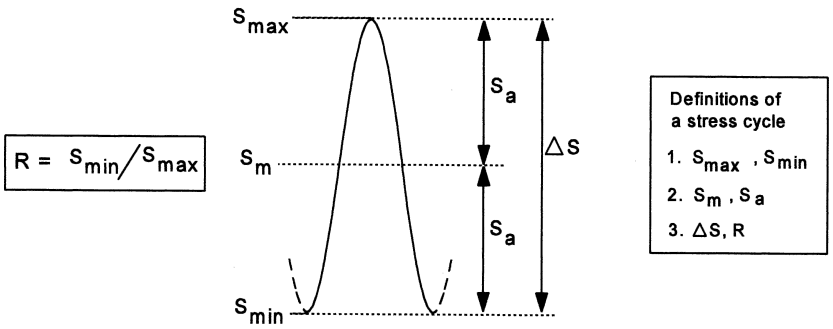

Fig. 6.1 Characteristic stress levels of load cycle.

Which definition of a stress cycle should be preferred? From a fatigue mechanistic point of view the obvious choice is $S_{\max}$ and $S_{\min}$. Those are the stress levels at which the loading direction is reversed, and thus cyclic slip is reversed. Crack extension in a cycle stops at $S_{\max}$. However, in service, a structure quite often is carrying a stationary load with a superimposed cyclic load. The stationary load can be a result of the weight of the structure, cargo, etc. The stationary load accounts for the mean stress, whereas loads in service induce cycles with certain stress amplitudes. If the severity of the cyclic load spectrum can be reduced, the S_a-values becomes smaller but S_m remains the same. Another situation occurs if a designer wants to increase the fatigue life by reducing the design stress level, e.g. by increasing the cross section of the fatigue critical area. All stress levels are then reduced with the same ratio. In other words, the stress ratio R remains constant, but ΔS is reduced. All three definitions of a stress cycle are used in the literature on fatigue.

In addition to the stress levels, another characteristic involved in the definition of a stress cycle is the *wave shape of the cycle*. The influence of the wave shape was briefly touched upon in Section 2.5.7. Effects of the wave shape and cyclic loading rate (i.e. the frequency in cycles per minute) can be important if a time dependent phenomenon is affecting the fatigue mechanism. It can be corrosion or creep, and also diffusion mechanisms in the material. Such effects are not yet considered in the present chapter.

The various ways to describe fatigue properties of a material are discussed in this chapter. It includes the fatigue limit, S-N curves and fatigue diagrams, all related to unnotched specimens. This is done in Section 6.2. General aspects of the fatigue strength are discussed in Section 6.3 which includes the correlation of the fatigue limit for $S_m = 0$ with the material ultimate tensile stress, the effect of the mean stress, different types of loading (tension,

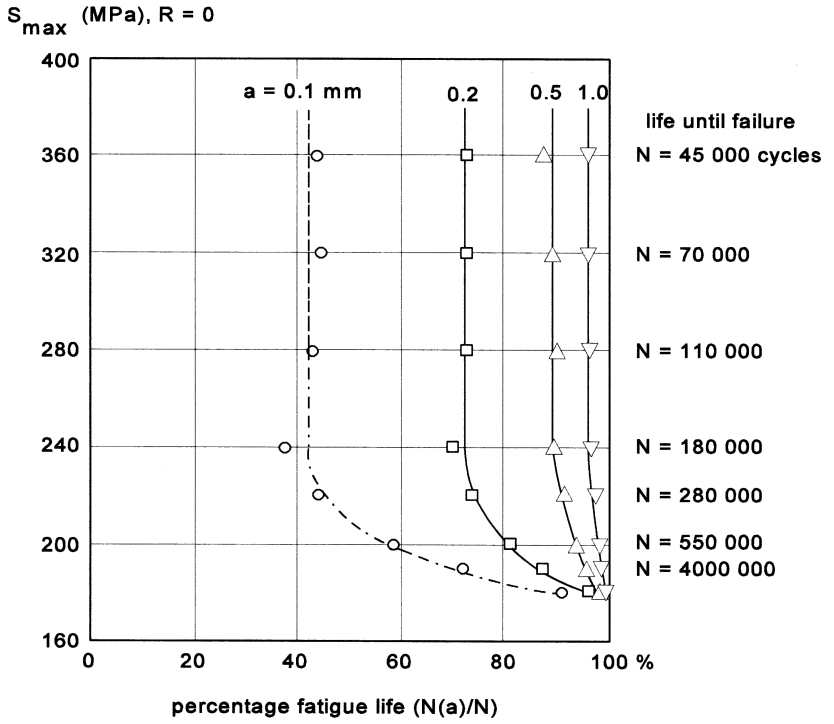

Fig. 6.2 The length of small cracks as a function of the percentage of life until failure. Results of unnotched specimens of an Al-alloy, 2024-T3 [1].

bending, torsion) and also combined loading. Low-cycle fatigue is addressed in Section 6.4. The main items of the present chapter are summarized in Section 6.5. The fatigue strength of notched specimens and predictions on the fatigue strength of notched elements are discussed in Chapter 7.

6.2 Description of fatigue properties of unnotched material

Fatigue properties of unnotched specimens are generally supposed to be material properties, such as S-N curves (fatigue lives until failure N), or the fatigue limit defined as the horizontal asymptote of an S-N curve. This information is coming from fatigue tests carried out until failure, or until a very high number of cycles if failure does not occur, e.g. 10^7 cycles. Observations on crack growth are not included. In Chapter 2, it was discussed that microcracks are nucleated early in the fatigue life which implies that the fatigue life covers two phases: (i) an initiation period including microcrack

growth, and (ii) a crack growth period with macro crack growth, see Figure 2.1. The second period is relatively short for unnotched specimens. Illustrative data are given in Figure 6.2 for unnotched specimens of an Al-alloy. Cracks as small as 0.1 mm were detected during continuous observations with binocular microscopes. For the higher fatigue stress levels, a crack of 0.1 mm occurred at about 40% of the fatigue life until failure. However, at 95% of the life the crack was still small, in the order of 1.0 mm. Such cracks cannot be seen with the unaided eye. In other words; the life until failure is only slightly larger than the crack initiation life, and practically almost the same.

The results in Figure 6.2 show another noteworthy trend. For low fatigue stress levels with fatigue lives in the order of 10^6 cycles and more, the curves for a constant crack length values go to 100% fatigue life. This illustrates that it becomes more difficult for microcracks to grow until failure if the stress level goes down to the fatigue limit. It confirms the threshold character of the fatigue limit.

A similar trend was already observed in the discussion on Figure 2.22 (Section 2.5.5) with the results of rotating beam specimens of mild steel. It was shown that the fatigue life until a crack of 2.5 mm was large if compared to the remaining life from 2.5 mm until failure. This was more obvious for the lower stress amplitude and the longer fatigue life. Although 2.5 mm is too large to be a microcrack, the trends agree with those of Figure 6.2 for the Al-alloy. It then seems reasonable to use S-N data of unnotched specimens for predictions on the crack initiation life of notched elements.

The S-N curve

An S-N curve, also called a Wöhler curve, is obtained as a result of a number of fatigue tests at different stress levels. An example of such results is given in Figure 6.3 for unnotched specimens of a CrMo steel (SAE 4130). In this tests $S_m = 0$, and thus the stress ratio is $R = S_{\min}/S_{\max} = -1$. The variable in Figure 6.3 is the stress amplitude S_a. The fatigue life N is usually plotted on a logarithmic scale. In the literature, the stress amplitude is presented both on a linear scale and on a logarithmic scale. Here, it is preferred to adopt the log scale because it frequently leads to an approximately linear relation between $\log S_a$ and $\log N$ for a substantial range of N-values. Mathematically, this linear relation can be written as

$$S_a^k N = \text{constant} \tag{6.2}$$

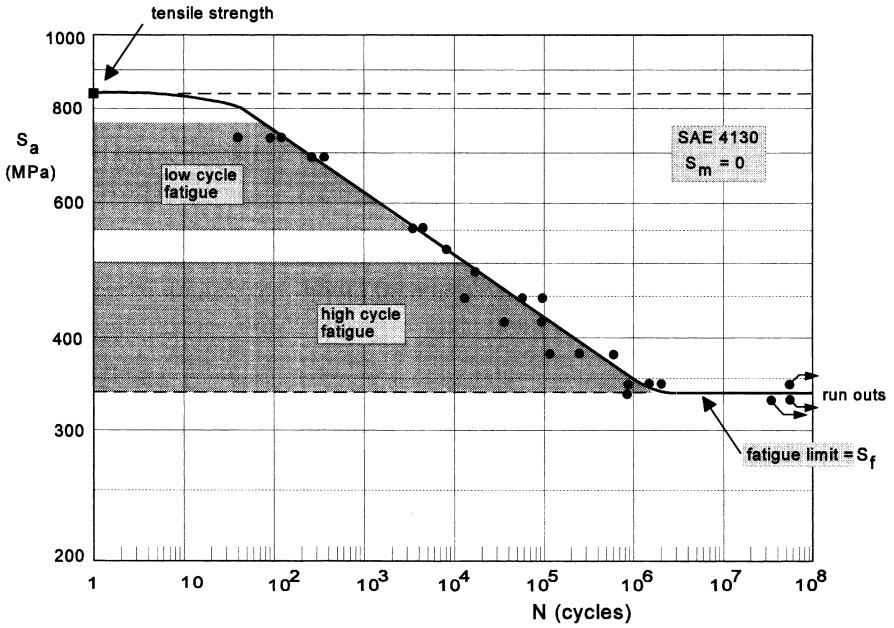

Fig. 6.3 Fatigue test results of unnotched specimens of a low-alloy steel (SAE 4130) [2].

The equation is known as the Basquin relation. The slope of the linear part is equal to $-1/k$. Some comments on Figure 6.3 should be made:

(i) Experiments carried out at the same S_a do not give the same fatigue life. Scatter between results of similar tests occurs. Three experiments at low stress amplitudes were stopped at 2.5 or 5×10^7 cycles without failure (so-called run outs). Scatter is the subject of Chapter 12.

(ii) The number of test results in Figure 6.3 is 25. The tests were run at a loading frequency of 30 Hz. Testing time for the experiments in the fatigue machine is in the order of 60 full days. Obviously, the simple S-N data in Figure 6.3 require an expensive test program.

(iii) In Figure 6.3 the lower horizontal asymptote is the fatigue limit S_f. However, a second horizontal asymptote occurs at the upper side of the S-N curve. If $S_{\max} = S_U$ (the tensile strength of the material), the specimen will fail in the first cycle as in a tensile test. For $S_m = 0$, this occurs if $S_a = S_U$, and for $S_m > 0$ if $S_a + S_m = S_U$. However, if S_a is slightly smaller, the specimen does not fail in the first cycle. Apparently, the specimen can then survive many cycles in the order of 100 or even more which is a result of strain hardening, see Figure 6.4. In the first uploading half cycle from O to A, a large plastic strain

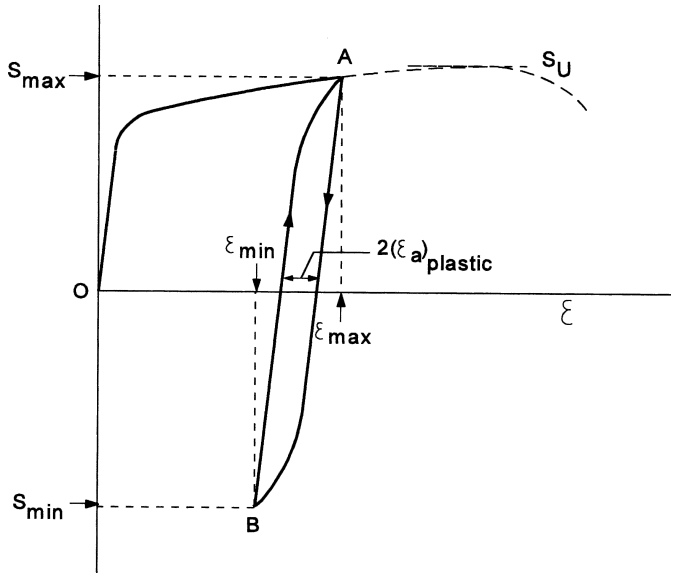

Fig. 6.4 Stress-strain loop of a high-stress amplitude cycle after the first application of S_{max}.

deformation occurs because S_{max} is exceeding the yield stress. But the following unloading to B and subsequent reloading to A cause a much smaller plastic strain amplitude due to plastic strain hardening of the material, see the hysteresis loop in Figure 6.4. The hysteresis loop can be sustained a substantial number of cycles before microcracking leads to failure. As a result, an upper horizontal asymptote is found. The situation is different if the specimen is not loaded under a constant stress amplitude, but under a constant strain amplitude as discussed in Section 6.4.

Fatigue at high amplitudes and fatigue lives up to some 10^4 cycles is called *low-cycle fatigue* (or high-level fatigue), see Figure 6.3. If fatigue covers a large number of cycles, say 10^5 cycles or more, it is called *high-cycle fatigue* (or low-level fatigue). The boundary between low and high-cycle fatigue is not exactly defined by a specific number of cycles. The more relevant difference between the two conditions is that low-cycle fatigue is associated with macroplastic deformation in every cycle. High-cycle fatigue is more related to an elastic behavior on a macro scale of the material. Actually, high-cycle fatigue is the more common case in practice, whereas low-cycle fatigue is associated with specific structures and load spectra. In Section 6.4, attention is paid to low-cycle fatigue as a material phenomenon. The topic returns in some later chapters.

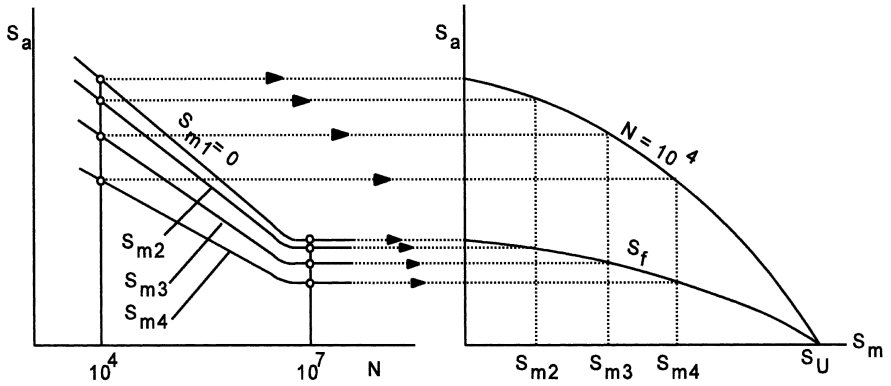

(a) S-N curves for different S_m-values

(b) Fatigue diagram lines derived from S-N curves

Fig. 6.5 Fatigue diagram as a cross plot of S-N curves.

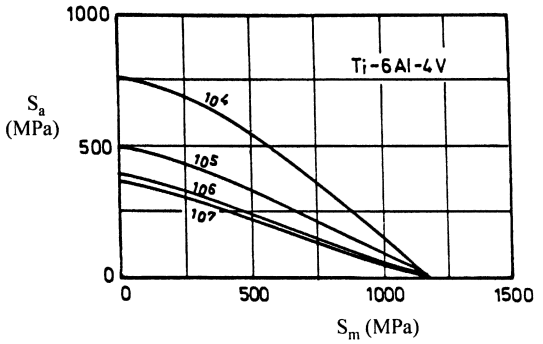

Fig. 6.6 Fatigue diagram of a Ti-alloy with lines for a constant fatigue life.

Fatigue diagrams

The mean stress for the S-N curve in Figure 6.3 is $S_m = 0$. Different S-N curves are obtained if fatigue tests are carried out at other S_m-values, see Figure 6.5a. A higher mean stress will give a lower S-N curve. Cross plots can now be made to arrive at a fatigue diagram with lines for a constant fatigue life as illustrated in Figure 6.5b for $N = 10^4$ and for the fatigue limit. Lines for other fatigue lives can be drawn in a similar way in the same diagram. An example of such a fatigue diagram is given in Figure 6.6 for a Ti-alloy. All lines for a constant N are converging to the same point on the S_m axis, $S_m = S_U$ for $S_a = 0$ (i.e., no cyclic stress) which theoretically should be expected. Fatigue diagrams generally suggest that the effect of S_m is not

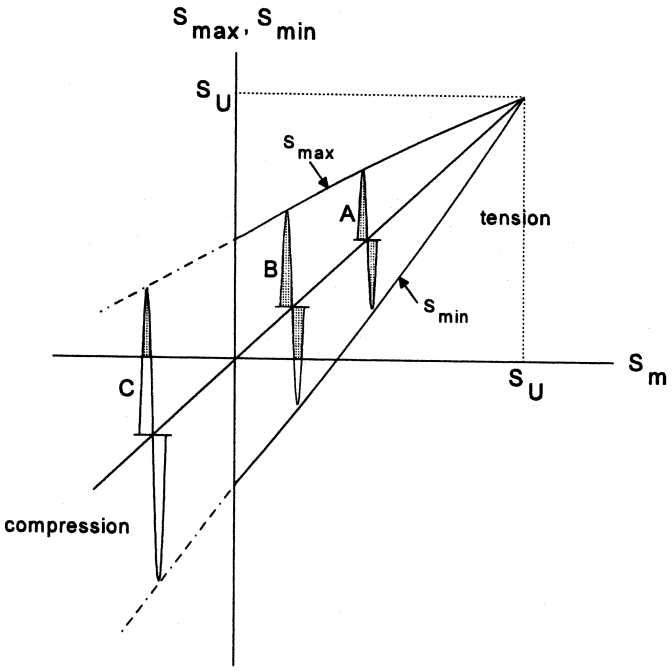

Fig. 6.7 Smith diagram. Lines for a constant N.

large, especially if N is high. It implies the general experience that *the stress amplitude S_a has a much larger effect on fatigue than the mean stress*. The trend reflects that fatigue is primarily a consequence of cyclic loads.

The fatigue diagram in Figure 6.6 is usually referred to as a Goodman diagram. Another way to present such data is offered by the Smith diagram where both $S_{\max}$ and $S_{\min}$ are plotted as a function of the mean stress S_m, see Figure 6.7. The two lines apply to one specific fatigue life, in many cases to a high fatigue life, e.g. 10^7 cycles, in order to represent the fatigue limit. Three load cycles for different S_m-values are indicated, A, B and C. In case A for a positive mean stress both $S_{\max}$ and $S_{\min}$ are positive. However, in case B for a lower S_m the minimum stress is negative (compression) although the larger part of the load cycle occurs still in tension. In case C with a negative mean stress, the larger part of the load cycle occurs in compression. A fatigue crack is closed under compression, and the negative part of the cycle should thus be expected to be non-damaging. Reversed loading is significant in view of reversed (crack tip) plasticity, but crack opening is necessary for crack extension and for reversed plasticity in the crack tip plastic zone. If a negative S_m is present, crack opening requires a larger S_a. In practice, it implies that

fatigue is rarely a problem for a negative mean stress. As a consequence, fatigue diagrams are usually given for positive mean stresses only.

Perhaps it should be recalled from Chapter 2 that compressive cyclic stresses can produce microcracks at the material surface as a result of cyclic slip. Cyclic slip primarily depends on the shear stress amplitude, and not on the tensile stress along the surface of the material. Some microcracking in slip bands at the material surface can occur. Under a cyclic compressive fatigue load, these cracks are not effectively opened at $S_{\max}$. As a result, microcracks will be non-propagating.

6.3 Some general aspects of the fatigue strength of unnotched specimens

Extensive literature is available on the fatigue strength of a material and how it is affected by various characteristics of the material and testing conditions. Some general aspects covered in this section are primarily discussed in relation to the effects on the fatigue limit. These effects are significant for the nucleation period and less important for the crack growth period. With reference to Figure 6.3, it can also be said that these effects are larger for *high-cycle fatigue* and relatively small for *low-cycle fatigue*. This is especially true for surface effects as discussed already in Section 2.5.5, see Figure 2.23.

Some classical topics associated with fatigue properties are:

- Relation between the fatigue limit, usually S_f for $S_m = 0$, and the strength of the material, in general the ultimate tensile strength, S_U.
- Mean stress effect.
- Size of the unnotched specimen.
- Type of loading; tension, bending, torsion.
- Combined loading, e.g. tension and torsion, or bending and torsion.
- Low-cycle fatigue.

6.3.1 Relation between S_f and S_U

An old idea is that the fatigue limit S_f can be increased by raising the strength of a material, either by the chemical composition of the alloy, or by a heat treatment which increases the hardness. Results for different C-steels

and low-alloy steels were already presented in Section 2.5.2. Figure 2.11 illustrates a systematic increase of S_f for an increasing S_U, but a good deal of scatter is present. Similar graphs are presented here in Figures 6.8 for cast iron, Al-alloys and Ti-alloys. They show a similar proportionality between S_f and S_U again with considerable scatter. If the proportionality is written as

$$S_f = \alpha S_U \tag{6.3}$$

then Figures 2.12 and 6.8 indicate $\alpha \approx 0.5$ for steel, cast iron and Ti-alloys, but a lower value $\alpha \approx 0.35$ applies to the Al-alloys. In comparison to the tensile strength, Al-alloys are more fatigue sensitive. The α-value can be adopted to make a first estimate of S_f for unnotched material ($K_t = 1$) at $S_m = 0$. In view of the scatter shown in Figures 2.12 and 6.8, Equation (6.3) gives a first estimate only. Moreover, it should be kept in mind that the fatigue limit of unnotched specimens with $S_m = 0$ is not necessarily a good measure for the fatigue resistance of a material. It does not give an indication of the fatigue sensitivity if notches are present. This problem is discussed in Chapter 7.

It is noteworthy that the fatigue limit in Equation (6.3) is related to the tensile strength. It seems to be more logical to relate S_f to the yield stress $S_{0.2}$. The tensile strength is depending on the strain hardening of the material after substantial plastic deformation has occurred. The yield stress is more characteristic for the small plastic strain behavior. Although an increased S_U is usually attended by a higher $S_{0.2}$, the correlation between the yield stress and the tensile strength is not a proportional relation. The origin of the relation $S_f = \alpha S_U$ is of a historical nature, but the reader should be aware that its physical meaning is limited.

6.3.2 Mean stress effects

If S_m is increased and S_a remains the same, then $S_{\max}$ becomes larger. As a result, a larger stress is present to open microcracks or macrocracks. A shorter fatigue life and a lower fatigue limit should thus be expected as illustrated by the fatigue diagram in Figure 6.6. Two simple equations have been proposed for the constant N lines in a fatigue diagram which in the literature are labeled as the modified Goodman relation and the Gerber parabola, see Figure 6.9. As should be expected, the fatigue strength is reduced to zero if the mean stress is increased to the ultimate tensile stress S_U. Any small S_a cycle at $S_m \approx S_U$ should immediate lead to failure

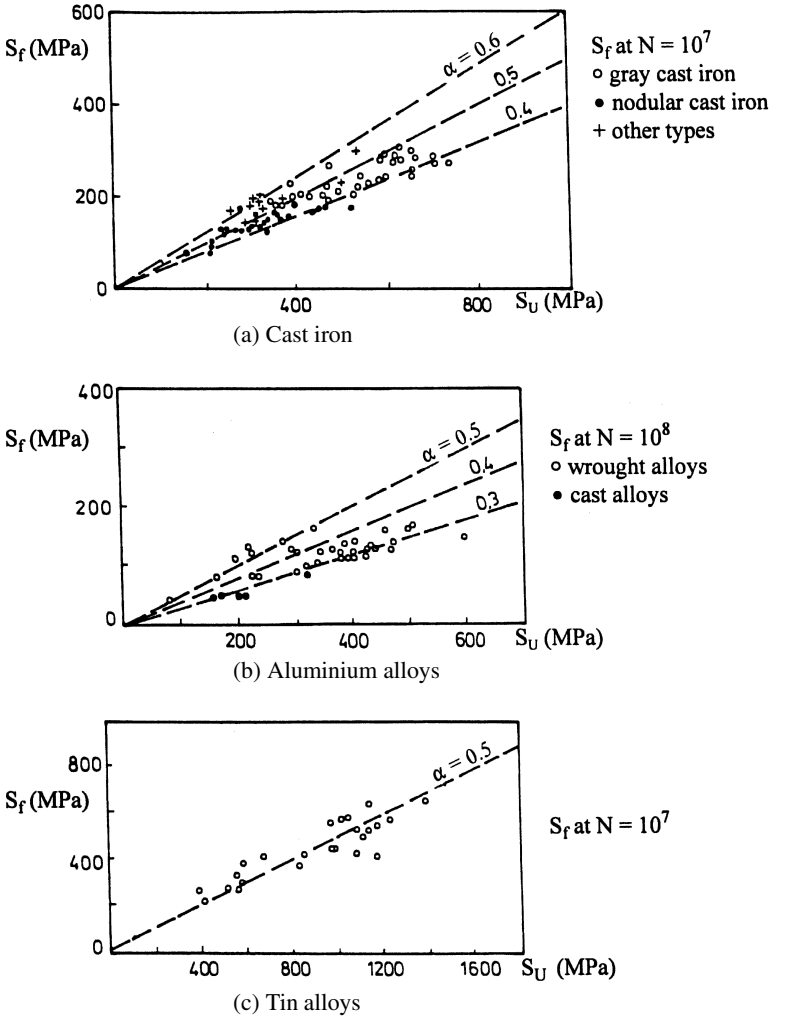

Fig. 6.8 Correlation between the fatigue limit and the tensile strength for different materials, see Figure 2.11 for steel [4].

because $S_{\max} > S_U$. The modified Goodman relation assumes a linear decrease of the fatigue strength for an increasing S_m. In many cases this approximation is conservative which is true for the Ti-alloy in Figure 6.6. However, exceptions occur, especially for high-strength alloys with a low ductility, see Figure 6.10 for AISI-4340 steel heat treated to the very high S_U of 1830 MPa. The fatigue strength drops more rapidly then according to the modified Goodman relation. This may well be due to the presence of small inclusions as discussed in Section 2.5.2.

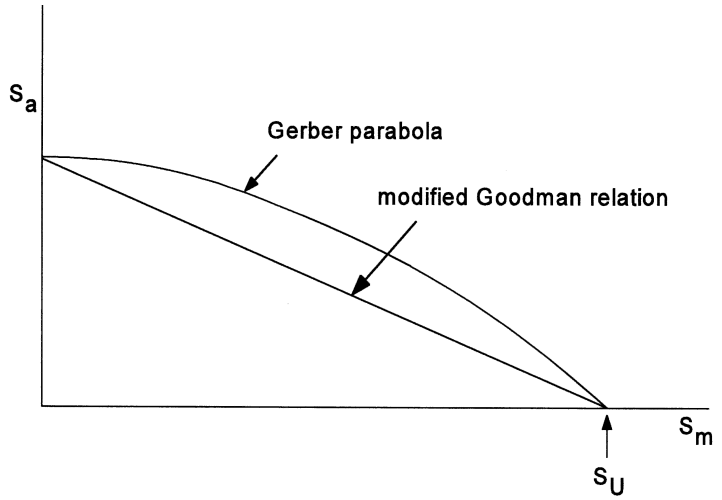

Fig. 6.9 Two approximations for constant N lines in a fatigue diagram.

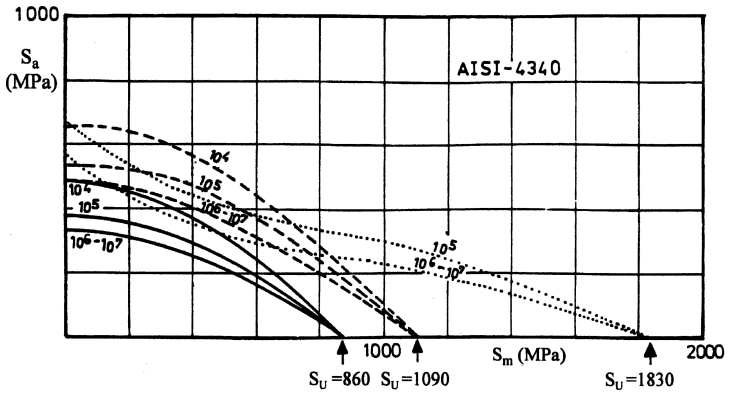

Fig. 6.10 Fatigue diagram for a low-alloy steel heat treated to three different S_U-values [3].

The Gerber parabola has its vertical axis along the S_a axis ($S_m = 0$). The parabola also passes through $S_m = S_U$ for $S_a = 0$. Denoting the fatigue strength for a certain fatigue life by S_N, the Gerber parabola is

$$\frac{S_N}{(S_N)_{S_m=0}} = 1 - \left(\frac{S_m}{S_U}\right)^2 \tag{6.4}$$

For the Ti-alloy in Figure 6.6 the Gerber parabola is unconservative. But for AISI4340 the parabola is a reasonable approximation in Figure 6.10 for the alloy heat treated to lower S_U-values. In general, the Gerber parabola reflects

the effect of the mean stress better for ductile[11] materials and high N-values, thus also for the fatigue limit S_f. However, high-strength alloys with a low ductility are more sensitive for the mean stress. Schütz [5] analyzed this sensitivity for a variety of materials for which the fatigue limit was available at $S_m = 0$ and at $R = 0$ ($S_a = S_m$). With these two fatigue limits, he defined the mean stress sensitivity as the initial average slope of constant N lines, see Figure 6.11:

$$M = \tan\varphi = \frac{(S_N)_{S_m=0} - (S_N)_{R=0}}{(S_N)_{R=0}} \tag{6.5}$$

A larger M implies a higher S_m sensitivity. Schütz collected data for unnotched and notched specimen and for different N-values including a high N-value associated with the fatigue limit. A systematic S_m sensitivity was observed for different groups of materials. The average curves of Schütz are presented in Figure 6.11. It clearly shows the increased mean stress sensitivity for materials with a higher tensile strength.

6.3.3 The size effect for unnotched specimens

A size effect implies that larger specimens may have a lower fatigue strength. A size effect on the fatigue limit of unnotched specimens has indeed been observed in experimental programs. As an example results of fatigue tests are shown in Figure 6.12a for three steel grades. A higher S_f is found for rotating bending specimens with a smaller diameter. Another example for a Cr-steel is given in Figure 6.12b with the same trend for rotating bending. It also shows a significantly lower S_f for cyclic tension/compression ($S_m = 0$). As pointed out in Chapter 2, the fatigue limit is primarily a question of some specific weak spots for crack nucleation at the material surface (or just below the surface). It is a matter of scatter of favorable sites for microcrack nucleation. The probability of having such weak spots is larger for a larger material surface area carrying the maximum stress cycle. In other words; it sounds logical that a size effect is present, and that larger specimen will exhibit a lower fatigue limit. Also, the critical material surface area of an unnotched tension specimen loaded under cyclic tension/compression is relatively large if compared to a cantilever rotating bending specimen. It thus

[11] A material is referred to as being ductile if it allows substantial plastic deformation without failure. The ductility is associated with a reasonable elongation until failure in a static tensile test. The opposite of ductile is "brittle".

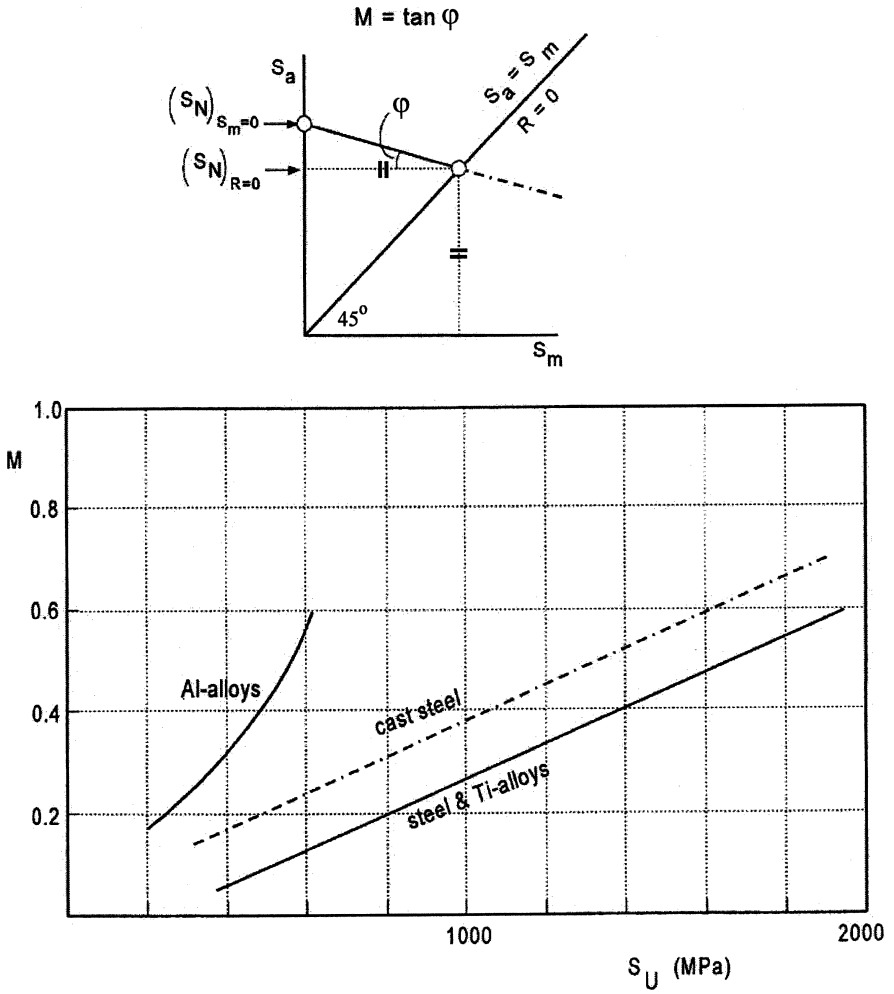

Fig. 6.11 Effect of the tensile strength on the influence of S_m on the fatigue strength S_N [5].

may be expected that the fatigue limit for cyclic tension in Figure 6.12b is lower than for cyclic bending.

Actually, the problem is more complex. Possible shapes for a flat and a cylindrical unnotched specimen are given in Figure 6.13. An unnotched specimen with $K_t = 1$ can theoretically be obtained in a prismatic specimen. However, specimens have to be clamped at both ends to transmit the load of the fatigue machine into the specimen. As a consequence, a stress concentration at the ends cannot be avoided. But the transition from the clamping area to the test section should be made as smooth as possible to

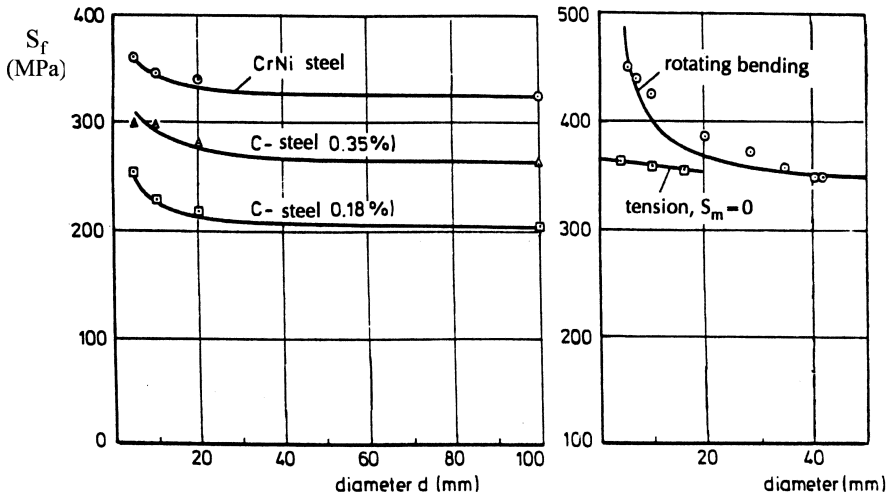

(a) Rotating bending

(b) Rotating bending and cyclic tension, 1.05 Cr-steel

Fig. 6.12 Size effect on the fatigue limit of different types of steel [6, 7].

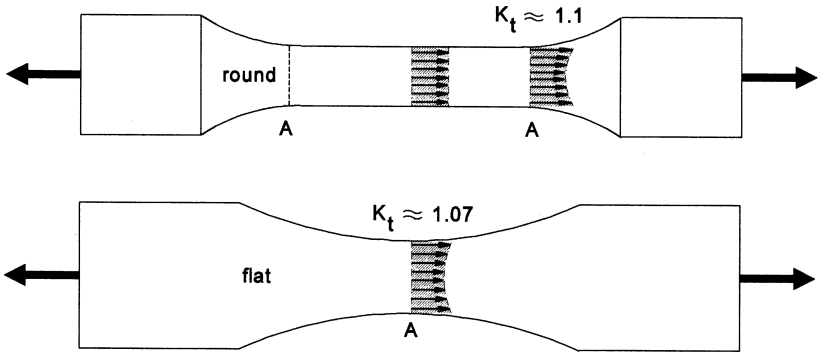

Fig. 6.13 Stress distributions in unnotched specimens.

keep K_t close to 1.0. The K_t-values for the two shapes shown in Figure 6.13 are 1.10 and 1.07 respectively. The round specimen in Figure 6.13 has a large cylindrical part, but the nominal stress in this part is about 10% lower than the peak stress in the two cross sections A. The peak stress in the flat specimen, $1.07S_{\text{nominal}}$, occurs in the minimum section A only. Fatigue failure will occur near this section A.

Another difference between the two specimens in Figure 6.13 should also be recognized. In the round specimen, the peak stress occurs all around the two cross sections A. However, in the flat specimen it occurs at the edges in cross section A. In the rectangular cross section, cracks often nucleate at the

corners because the restraint on cyclic plasticity is minimal at those corners. It must be concluded that the fatigue strength, and in particular the fatigue limit is depending on *the size and the shape of the specimen*. It implies that the fatigue limit of unnotched specimens, which is considered to be a fundamental property of a material, is not really such a well defined property. The question may then be raised for which practical reasons should we be interested in fatigue properties of unnotched specimens? Several reasons for a limited significance of the fatigue limit can be mentioned.

(i) *Material selection*. Because fatigue properties of unnotched specimens depend on the size and the shape of the specimen, material fatigue data of these specimens can only be used to obtain approximate ideas about the fatigue resistance of a material. But it should be kept in mind that basic data for unnotched specimens do not give indications about the fatigue notch sensitivity of a material.

(ii) *Comparative testing*. Because the fatigue properties of unnotched specimens depend heavily on the surface conditions of the specimens, comparative testing can certainly be done on unnotched specimen, e.g. to compare different surface treatments, e.g. nitriding of steel. Care should still be taken that the size and the shape of the specimen are sufficiently representative for the intended practical application of a surface treatment. In other words, a more relevant approach is to perform comparative tests on specimens with a notch geometry and a surface quality representative for the practical application.

(iii) *Prediction of fatigue properties of notched elements*. The old idea is that fatigue properties of notched elements can be predicted starting from the fatigue properties of unnotched specimens as basic material data. It assumes that the conditions for crack nucleation in notched elements and in unnotched specimens can be similar. In view of the preceding discussion on size and shape effects, this is no longer so obvious. Predictions of the fatigue properties of notched elements is a most relevant question for designing against fatigue. This topic is addressed in Chapter 7.

6.3.4 Type of loading, tension, bending, torsion

In the previous sections it was tacitly assumed that fatigue occurs under cyclic tension or cyclic bending. Fatigue under cyclic tension and under cyclic bending are not that much different. The critical stress of an unnotched

Table 6.1 Fatigue limit ratios.

Material	Mean value of τ_f/S_f
Steel	0.60
Al-alloys	0.55
Cu and Cu-alloys	0.56
Mg-alloy	0.54
Ti	0.48
Cast iron	0.90
Cast Al- and Mg-alloys	0.85

specimen in both cases is cyclic tension in the surface layer of the material. The stress gradient perpendicular to the material surface is different for tension and bending, but as discussed in Section 3.3 the more important stress gradients occur along the material surface.

The occurrence of fatigue under cyclic torsion was mentioned in Chapter 2, see Figures 2.31 and 2.32. Classical examples of fatigue under cyclic torsion are associated with axles and spiral springs. Nucleation of the first microcrack again occurs in slip bands carrying the maximum shear stress. This shear stress amplitude in an unnotched specimen loaded in tension is equal to half the tensile stress, or $\tau_a = S_a/2$. For an unnotched specimen, loaded under cyclic torsion, the maximum shear stress is equal to the shear stress on the specimen. As a first estimate, one might expect that the fatigue limit under cyclic torsion, τ_f, is half the fatigue limit S_f under cyclic tension in agreement with the Tresca yield criterion. However, as indicated in Figure 2.31, such slip bands under cyclic tension are also loaded by a tensile stress perpendicular to the slip bands, whereas this tensile stress is absent for cyclic torsion. As a result, the conversion of cyclic slip into a microcrack may be more difficult under cyclic torsion, and τ_f may be larger than $S_f/2$. Data from the book of Forrest [4] are given in Table 6.1.

The τ_f/S_f ratios for the wrought alloys, ignoring the value for Ti, are close to the ratio predicted by the Von Mises criterion ($0.577 = 1/\sqrt{3}$). Actually, physical reasons why that criterion should be applicable are questionable if crack nucleation is associated with cyclic slip. A noteworthy result is the high τ_f/S_f ratios for the cast alloys. Consider grey cast iron with the graphite flakes as the starter notches for microcracks. The flakes are depicted in Figure 6.14 as very flat defects with some random orientation. It implies that the maximum peak stress at the ends of the flakes will have an equivalent character for pure tension and for pure torsion. The fatigue limits S_f and τ_f might then be equal. The τ_f/S_f ratio of 0.9 is indeed close to 1.

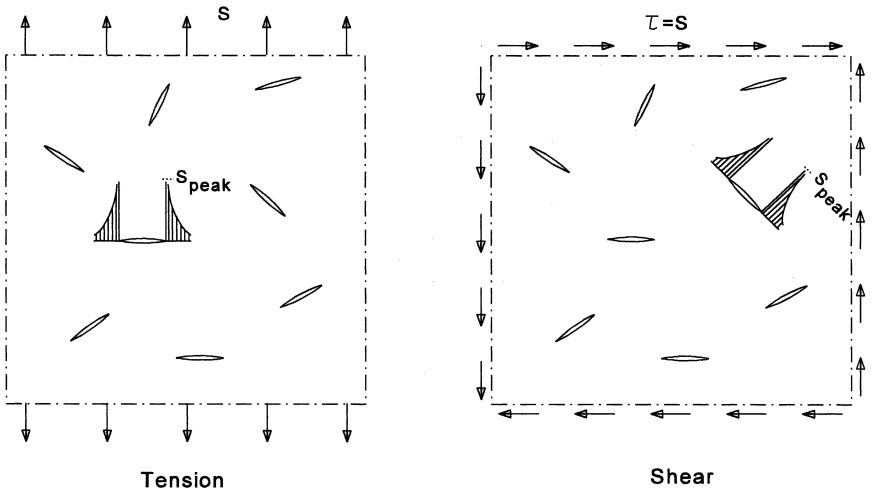

Fig. 6.14 Peak stress at flat material defects in cast iron (graphite flakes). Similarity between tension and shear, same peak stress.

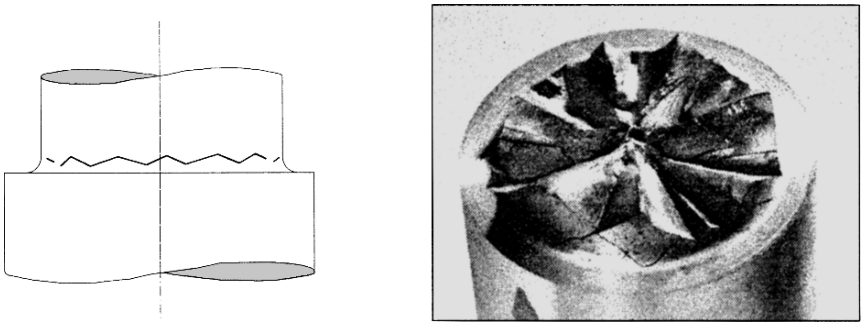

Fig. 6.15 Fatigue failure obtained under cyclic torsion ($\tau_a = 150$ MPa) in a round specimen with a fillet notch, material carbon steel (0.45%C). Factory roof type fracture surface [9].

Similarly, the high τ_f/S_f ratio of the cast light alloys may also be associated with defects in the material.

The mean stress under cyclic torsion, τ_m, should not be expected to have a significant influence on cyclic slip. If this is true, τ_m should not affect crack nucleation. As a consequence, the fatigue limit, τ_f, should hardly depend on the mean stress τ_m. Experiments, noteworthy by Smith [8], have confirmed this behavior. However, a problem arises as a finite life is involved. Fatigue cracks grow preferably in a direction perpendicular to the main principal stress. This leads to a spiral crack growth in a cylindrical bar as shown in Figure 2.32. The crack started from a surface defect.

A fatigue failure in a non-cylindrical specimen starts in the minimum cross section where the nominal shear stress has its maximum. Spiral crack growth then would imply that the crack front will move away from the minimum section to areas with a lower nominal shear stress. Moreover, crack growth in the depth direction is also difficult in view of the decreasing shear stress. The problematic crack growth stimulates crack nucleation at other places in the root area of the notch. As a result of more simultaneously growing fatigue cracks a so-called factory roof failure is observed. An example is shown in Figure 6.15. Due to the geometrical shape of the radial ridges, some interlocking between the two fracture surfaces occur under torsional load. The complexity of the phenomenon obstructs a reasonable approach to predictions of fatigue lives.

6.3.5 Combined loading

Fatigue under combined loading is a complex problem. A rational approach might be considered again for fatigue crack nucleation at the material surface. The state of stress at the surface is two-dimensional because the third principal stress perpendicular to the material surface is zero. The most simple combination of loads is biaxial tension which occurs in pressurized vessels. It consists of two perpendicular tensile stresses. Such a loading case cannot be easily simulated on simple specimens, especially for unnotched material.

Another relatively simple combination of different loads is offered by an axle loaded under combined bending and torsion. This combination can be simulated in experiments, and test programs were reported in the literature. Early tests were carried out by Gough et al. [10]. They considered the fatigue limit and found a systematic effect of the combination of a bending stress amplitude and a torsional stress amplitude for which they proposed the elliptical quadrant criterion:

$$\frac{S^2}{S_f^2} + \frac{\tau^2}{\tau_f^2} = 1 \tag{6.6}$$

In this equation, S_f and τ_f, are the fatigue limits for single load cases, i.e.for pure tension and pure torsion respectively. They are supposed to be material constants. The criterion apparently agreed with test results for different materials. Results for some types of steel are presented in Figure 6.16. Equation (6.6) was less successful for cast alloys.

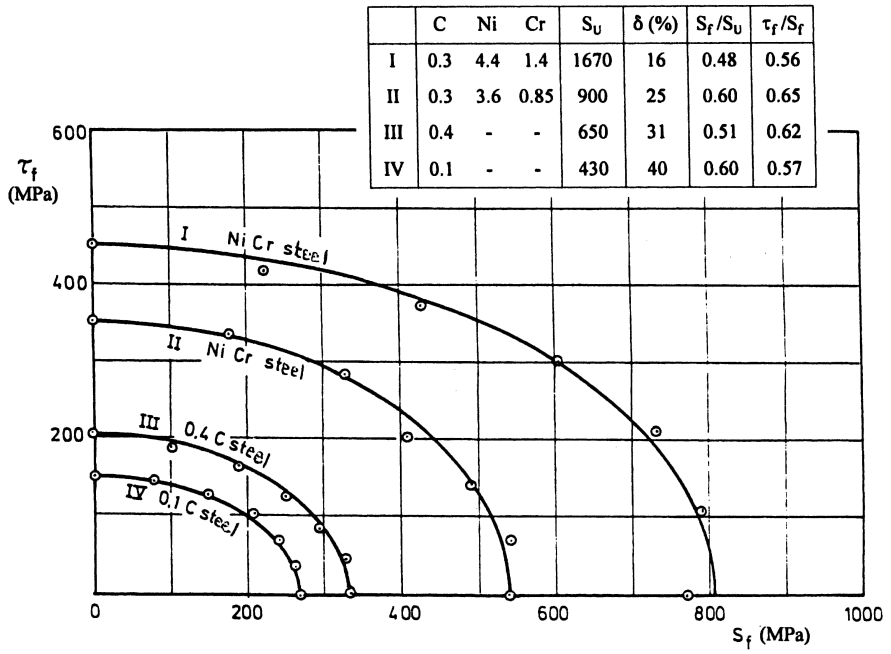

	C	Ni	Cr	S_u	δ (%)	S_f/S_u	τ_f/S_f
I	0.3	4.4	1.4	1670	16	0.48	0.56
II	0.3	3.6	0.85	900	25	0.60	0.65
III	0.4	-	-	650	31	0.51	0.62
IV	0.1	-	-	430	40	0.60	0.57

Fig. 6.16 The fatigue limit under combined tension and torsion (zero mean stress) [11].

The Von Mises criterion also predicts an elliptical quadrant equation for the 2D condition at the material surface. Actually, Equation (6.6) would become in full agreement with the Von Mises criterion if the ratio τ_f/S_f would agree with the Von Mises prediction (ratio 0.577). As said before, this is approximately true for several materials.

Combined loading in experimental programs has also been simulated by using tubular specimens which were loaded simultaneously in tension, in torsion and by internal pressure. Problems were encountered because the material used was not always isotropic. Tubular specimens are usually made of rod material which in many cases have a fibrous structure with elongated grains and impurities. Crack nucleation is sensitive to this kind of anisotropy. Secondly, crack growth observations were usually not made in such experiments. The test result was the number of cycles until failure or until a crack had penetrated through the full thickness of the wall of the tubular specimen. It should be realized that stress functions to account for combined stress conditions can only work for crack nucleation, i.e. for the fatigue life until the first microcrack has been created. As soon as crack growth occurs beyond the crack nucleation period, the stress condition becomes essentially different. Only if the crack growth period is very small

compared to the crack nucleation period, functions like Equation (6.6) can be meaningful.

In the previous paragraphs it was tacitly assumed that the combined cyclic loads occur with the same frequency and phase angle. This obviously is true for the biaxially loading of a pressure vessel. However, a different situation can apply to dynamically loaded components subjected to two different types of cyclic loads. As an example consider an axle transmitting a torsional moment with slow variations of the magnitude of this moment. The same axle is simultaneously loaded by a high frequency bending moment. A case which may be relevant for axles of propellers. Other complex combinations can occur in several structures, e.g. motor cars.

Theories for combined fatigue loads with different frequencies and phase angles are discussed in the literature, see e.g. [12, 13]. If fatigue failures should not occur, a fatigue limit criterion must be adopted again. It may be recalled that the fatigue limit is associated with crack nucleation due to cyclic slip. Cyclic shear stresses at the material surface have to be considered. In theory, these stresses can be calculated for combined loading systems. However the orientation of the most critical slip plane for out-of-phase fatigue loads is not a priory known. Furthermore, a critical shear plane will not carry a cyclic shear stress only, but also a tensile stress which need not be in phase with the cyclic shear stress. This tensile stress can affect the nucleation of a microcrack in a slip band. Fatigue crack initiation under out-of-phase fatigue loads is still a topic of research which unfortunately is not easily validated by experimental data.

As soon as a fatigue crack has been initiated, the loading system for crack growth is significantly affected. The fatigue crack may be expected to grow perpendicular to the main principle stress, but unfortunately this stress can have a varying direction The prediction of crack growth becomes a complex problem.

6.4 Low-cycle fatigue

Low-cycle fatigue as a phenomenon has received much attention since the early work of Coffin and Manson in the fifties and the sixties. It became clear that low-cycle fatigue is a problem which is different from high-cycle fatigue. As pointed out before, the high-cycle fatigue mechanism on a macro scale occurs as an elastic phenomenon. However, in low-cycle fatigue, macroscopic plastic deformation occurs in every cycle.

Low-cycle fatigue can be relevant to structures that are subjected to small numbers of load cycles in their economic life. If it would be required to keep all stress levels below a fatigue limit, the structure may become very heavy without this being necessary. An example of a structure for which low-cycle fatigue can be important is a pressure vessel that is pressurized only a small number of times in many years. Other examples are power generator structures with an elevated operation temperature and significant thermal stresses. The number of on/off conditions can be low and low-cycle fatigue should be considered. Moreover, if thermal stresses occur due to differential thermal expansions, the nature of the loading is cyclic strain rather than cyclic stress.

Under low-cycle fatigue, failure can occur in a small number of cycles, say 1000 cycles or less. Small cracks are usually nucleated immediately. In view of the high stress level, final failure will occur when the cracks are still small. Periods of visible crack growth are hardly present. In the discussion on Figure 6.4, it was pointed out that low-cycle fatigue under constant-amplitude loading leads to a high plastic deformation in the first cycle followed by much smaller strain amplitudes in subsequent cycles. For that reason, it is instructive to study the low-cycle fatigue process in the laboratory by imposing constant strain cycles on a specimen. In general, this loading condition is also representative for the low-cycle conditions in structures. Such tests can be performed on closed-loop fatigue machines with a feedback signal obtained from the strain in the specimen.

The stress amplitudes under constant strain cycles can vary during successive cycles. This is illustrated in Figure 6.17. In the upper part of this figure, the strain cycles require an increasing stress amplitude. *Cyclic strain hardening* occurs which is more common for initially soft materials. In the lower part of Figure 6.17 the opposite occurs. The strain cycle can be maintained with a decreasing stress amplitude which is referred to as *cyclic strain softening*. It primarily occurs in materials which are already hardened to a significant level, either by a heat treatment or a deformation process. If cyclic deformations are applied to such a material, it can trigger structural changes which lead to some relaxation of the potential energy in the matrix of the material. The material becomes softer. In general, both cyclic strain hardening and cyclic strain softening stabilize to a constant level after a number of cycles, usually a low number compared to the fatigue life until failure. Some materials are practically stable almost immediately, which applies to several high-strength materials if the high strength is obtained by a heat treatment. Stabilizing is less predictable for soft materials and materials strain hardened by a deformation process.

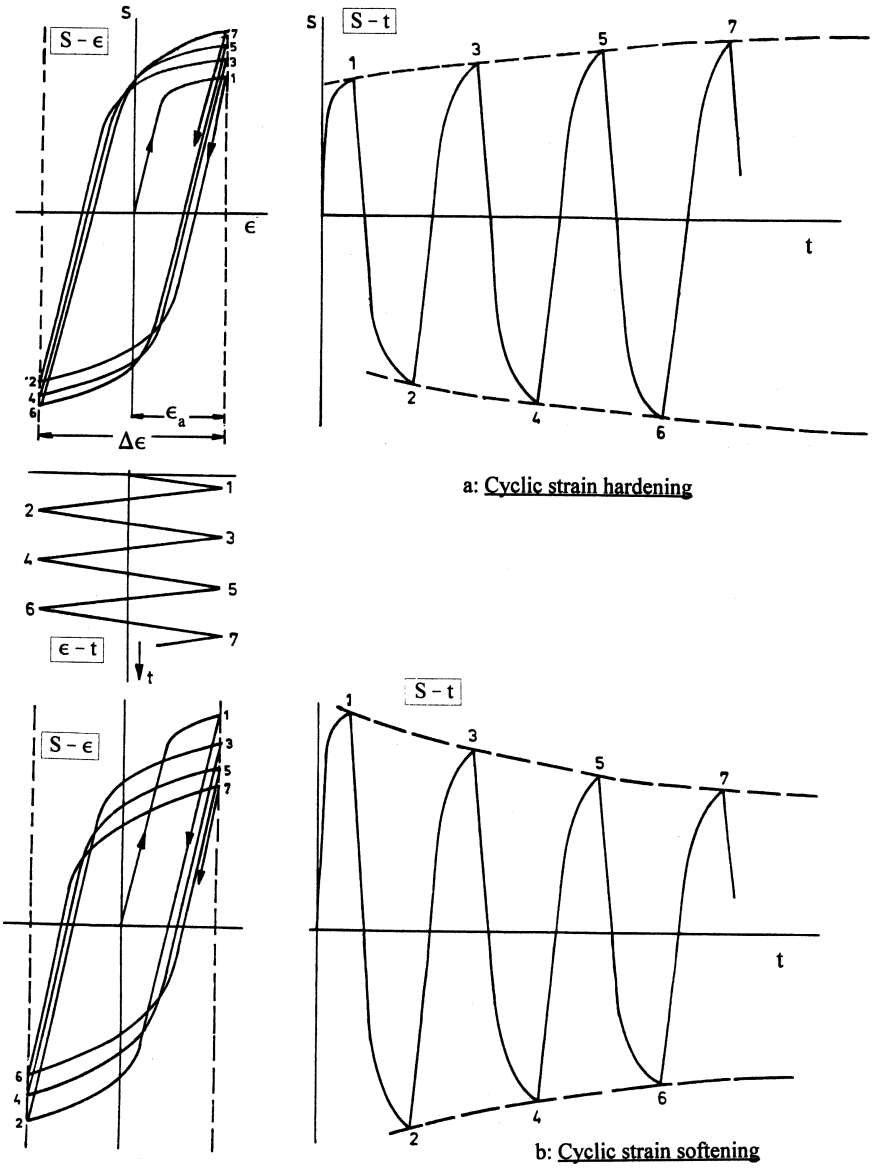

Fig. 6.17 Stress-strain loops during constant ε_a cycles of low-cycle fatigue, and the stress history for cyclic strain hardening and softening.

Coffin and Manson (independently) observed that the fatigue life under low-cycle fatigue conditions plotted as a function of the strain amplitude, ε_a, indicates a linear relation if plotted on a double logarithmic scale, see Figure 6.18. The relation can be written as:

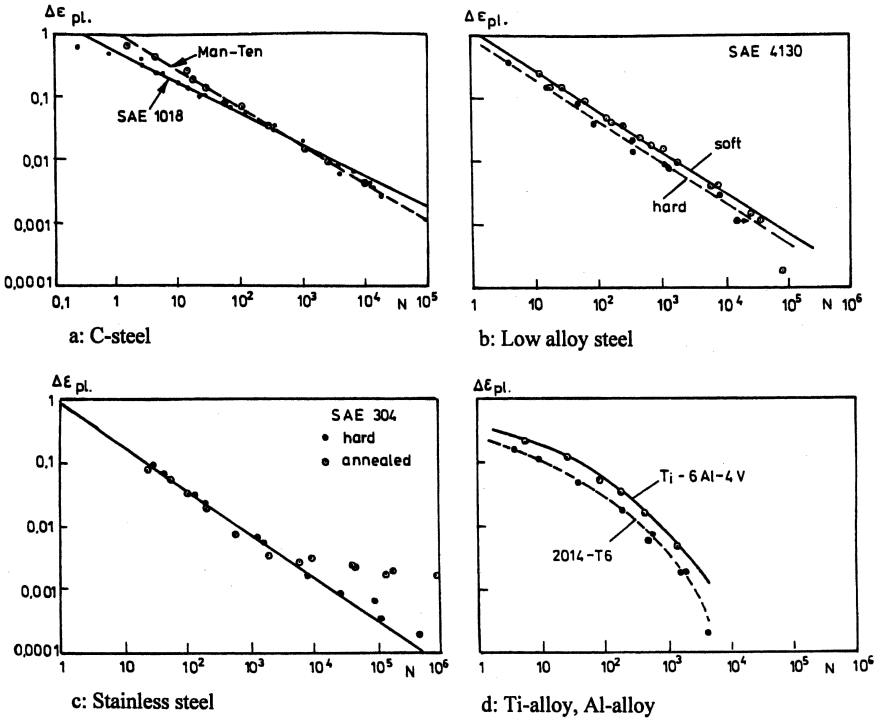

		(MPa) $S_{0.2}$	S_U
SAE 1018 Man-Ten	0,18 C (annealed) 0,23 C, 1,6 Mn	325	565
SAE 4130 soft	0,30 C, 0,95 Cr 0,20 Mo	780	897
hard		1360	1428
SAE 304 soft	0,03 C, 18,7 Cr, 8,5 Ni	255	745
annealed		745	952
Ti-6-4	6,1 Al, 4 V	1186	1235
2014-T6	4-5 Cu, 0,5 Mg, 1 Fe	462	510

Fig. 6.18 Low-cycle fatigue curves, N-$\Delta epsilon_{pl}$ ($\Delta\varepsilon_{pl} = 2\varepsilon_{a,pl}$) [16–18].

$$\varepsilon_a N^{\beta} = \text{constant} = C \quad \text{or} \quad \varepsilon_a = CN^{-\beta} \tag{6.7}$$

This equation is known as the Coffin–Manson relation. As shown by Figure 6.18, the relation appears to be satisfactory for several materials with two exceptions in the lower right graph. The exponent β quite often is in the order of -0.5.

It is noteworthy that the upper horizontal asymptote of the S-N curve at $S_{\max} = S_U$ (see Figure 6.3) is no longer present in the ε-N diagrams. It thus seems logical to correlate low-cycle fatigue life to the strain amplitude. Note

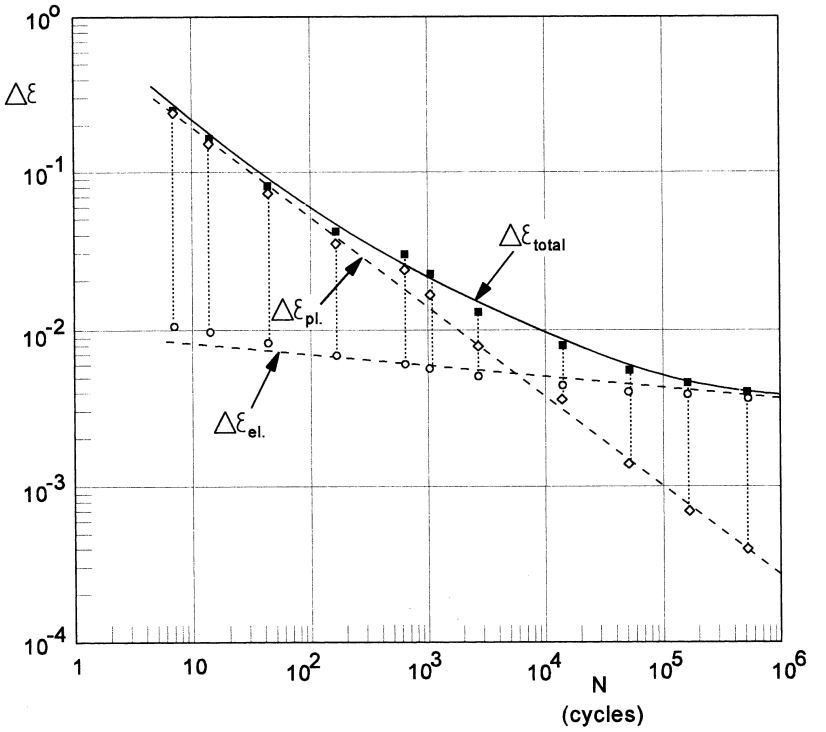

Fig. 6.19 Total strain range as the sum of the plastic and the elastic strain range. Material: AISI 4340 (annealed) [19]. (Range $\Delta\varepsilon = 2\varepsilon_a$)

the similarity between the Coffin–Manson relation and Basquin equation (Equation 6.2). Physical arguments underlying the Coffin–Manson relation appear to be questionable.

The Coffin–Manson relation can obviously not apply to high-cycle fatigue. The lower horizontal asymptote, i.e. the fatigue limit, is not covered by Equation (6.7).However, Manson and Hirschberg [15] considered also the elastic strain amplitude by a similar exponential relation to the fatigue life which lead to

$$\varepsilon_{a,\text{total}} = \varepsilon_{a,pl} + \varepsilon_{a,el} = C_1 N^{-\beta_1} + C_2 N^{-\beta_2} \tag{6.8}$$

Figure 6.19 shows the result for a stainless steel. The curve for $\varepsilon_{a,\text{total}}$ becomes non-linear with a tendency to bend towards a more horizontal direction at high endurances where the elastic strain amplitude predominates. Note that the description of the ε-N curve now asks for four material constants. Note also from Figure 6.19 that the elastic component ε_{el} for

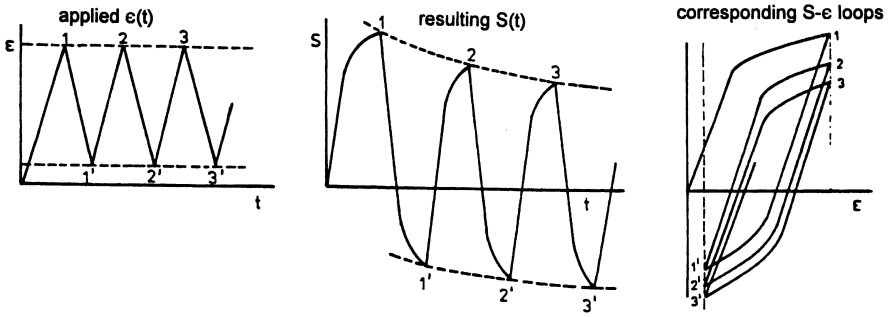

Fig. 6.20 Plastic shake-down, or stress relaxation.

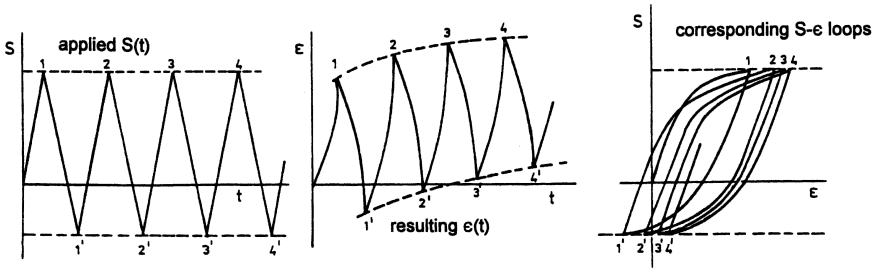

Fig. 6.21 Cyclic creep.

low lifetimes is negligible compared to the plastic one. Equation (6.8) might give a reasonable description of the ε-N curve of unnotched material if a fairly rapid stabilization of cyclic plasticity occurs. The question remains how useful it can be for prediction problems.

Plastic shake-down and cyclic creep

Two phenomena closely related to the occurrence of macroscopic cyclic plasticity should be mentioned here. Plastic shake-down can occur under cyclic plastic deformation if a positive mean strain is present, see Figure 6.20. During the cyclic deformations, the mean stress decreases, possibly to zero. This stress relaxation can occur because of dislocation rearrangements enabled by active cyclic slip. Residual stresses in a surface layer of a material can vanish if cyclic plastic deformation occurs in that layer. It generally requires relatively high cyclic stress levels.

A related phenomenon is cyclic creep occurring under a high cyclic stress with a positive mean stress, see Figure 6.21. The cyclic plastic

deformations are partly used for permanent tensile deformations. As a dislocation mechanism, it is related to plastic shake-down because the cyclic slip tries to invoke plastic shake-down. However, under a cyclic tensile stress with a positive mean value, shake-down of the mean stress cannot be successful. The material becomes longer; creep occurs. If cyclic strain hardening is effective, as suggested in Figure 6.21, creep will stop after a number of cycles. If strain hardening does not occur, it may well lead to continued creep until failure.

6.5 Main topics of the present chapter

1. Fatigue limits and S-N curves for unnotched specimens are generally supposed to be basic material properties. However, it should be recognized that these properties depend on the size and the shape of the unnotched specimens used, and also on the surface finish of the specimens. This is especially relevant to the fatigue limit because this property is mainly controlled by nucleation of microcracks at the material surface.
2. For a group of similar alloys, the fatigue limit of unnotched specimens (S_{f1}) for $S_m = 0$ increases with the ultimate tensile strength of a material if the higher strength is obtained by changing the alloy composition or an other heat treatment. As a first estimate for the fatigue limit, the linear relation $S_{f1} = \alpha S_U$ can be used with a characteristic α-value for a group of similar materials.
3. A large part of the S-N curve can be approximated by the Basquin relation, $S_a^k N =$ constant, a linear relation on a double log scale.
4. The fatigue properties on unnotched material can be described by fatigue diagrams. Lines for constant fatigue lives in such a diagram can be approximated by the Gerber parabola or by the modified Goodman relation. The Gerber parabola agrees more with the results of materials with a reasonable ductility whereas the modified Goodman relation is more applicable to the high-strength low-ductility materials.
5. The effect of the stress amplitude is more significant for the fatigue properties of a material than the effect of the mean stress, especially for high fatigue lives and the fatigue limit. The mean stress effect for different materials can be characterized by the slope factor M defined by Schütz (Figure 6.11). It indicates an increasing mean stress effect for an increasing strength of a material.

6. Fatigue is less significant for a compressive mean stress.
7. Fatigue under cyclic tension and cyclic bending is a similar phenomenon. However, under cyclic torsion it is different, both for crack nucleation and crack growth. The fatigue limit under cyclic torsion hardly depends on the mean shear stress.
8. For combined loading cases, e.g. cyclic bending and torsion, the fatigue limit can be described by an empirical relation. Complex problems are offered if combined loadings occur out of phase.
9. High-cycle fatigue and low-cycle fatigue refer to a significantly different behavior of the material. Under high-cycle fatigue, the material response is still macroscopically elastic. The fatigue life of specimens then is largely dominated by the crack initiation period while the crack growth period is relatively short. For low-cycle fatigue, macroscopic plasticity occurs in every cycle. Fatigue cycles should then be expressed in terms of strain amplitudes instead of stress amplitudes.

References

1. Schijve, J., *Significance of fatigue cracks in micro-range and macro-range.* Fatigue Crack Propagation, ASTM-STP 415 (1967), pp. 415–459.
2. Grover, H.J., Bishop, S.M. and Jackson, L.R., *Fatigue strength of aircraft materials. Axial load fatigue tests on unnotched sheet specimens of 24S-T3, 75S-T6 aluminum alloys and of SAE 4130 steel.* NACA TN 2324 (1951).
3. Grover, H.J., *Fatigue of Aircraft Structures*. U.S. Government Printing Office (1966).
4. Forrest, P.G., *Fatigue of Metals*. Pergamon Press, Oxford (1962).
5. Schütz, W., *View points of material selection for fatigue loaded structures*. Laboratorium für Betriebsfestigkeit LBF, Darmstadt, Bericht Nr. TB-80 (1968) [in German].
6. Buch, A., *Evaluation of size effects in fatigue tests on unnotched specimens and components*. Arch. Eisenhüttenwesen, Vol. 43 (1972), pp. 885–900 [in German].
7. Kloos, K.H., Buch, A. and Zankov, D., *Pure geometrical size effect in fatigue tests with constant stress amplitude and in programme tests.* Zeitschr. Werkstoftechn., Vol. 12 (1981), pp. 40–50.
8. Smith, J.O., *Effect of range of stress on fatigue strength.* University of Illinois, Engrg. Expt. Station Bulletin 334 (1942).
9. Leger, J., *Fatigue life testing of crane drive shafts under crane-typical torsional and rotary bending loads*. *Schenck Hydropuls Mag.*, Issue 1/89 (1989), pp. 8–11.
10. Gough, H.J. and Pollard, H.V., *The strength of metals under combined alternating stresses.* Proc. Inst. Mech. Engrs, Vol. 131 (1935), pp. 3–103.
11. Gough, H.J. and Pollard, H.V., *Some experiments of the resistance of metals to fatigue under combined stresses.* Min. of Supply, Aero Res. Council, RSM 2522, Part I (1951).
12. Ballard, P., Dang Van, K. Deperrois, A. and Papadopoulos, Y.V., *High cycle fatigue and a finite element analysis.* Fatigue Fracture Engrg. Mater. Struct., Vol. 18 (1995), pp. 397–411.
13. Socie, D. and Marquis, G.B., *Multiaxial Fatigue*, John Wiley & Sons (1999).

14. Coffin Jr., L.F., *Low cycle fatigue – A review.* Appl. Mater. Res., Vol. 1, No. 3 (1962), p. 129.
15. Manson, S.S. and Hirschberg, M.H., *Fatigue behavior in strain cycling in the low- and intermediate-cycle range*. In Fatigue, An Interdisciplinary Approach, J.J. Burke, N.L. Reed and V. Weiss (Eds.). Syracuse University Press (1964), p. 133.
16. Coffin Jr., L.F. and Tavernelli, J.F., *The cyclic straining and fatigue of metals.* Trans. Metall. Soc. AIME, Vol. 215 (1959), pp. 794–807.
17. Brose, W.R., *Fatigue life predictions for a notched plate with analysis of mean stress and overstrain effects.* In Fatigue under Complex Loading, R.M. Wetzel (Ed.). SAE Advanced in Engineering, Vol. 6 (1977), pp. 117–135.
18. Smith, R.W., Hirschberg, M.H. and Manson, S.S., *Fatigue behavior of materials under stain cycling in low and intermediate life range.* NASA TN D1574 (1963).
19. Graham, J.F., *Fatigue Design Handbook.* Soc. of Automotive Engineers (1968).

General references

20. Sonsino, C.M., *Course of S-N-curves especially in the high-cycle fatigue regime with regard to component design and safety.* Int. J. Fatigue, Vol. 29 (2007), pp. 2246–2258.
21. Murakami, Y., *Metal fatigue: Effects of small defects and nonmetallic inclusions.* Elsevier (2002).
22. Stanzl-Tschegg, S.E. and Mayer, H.R., *Fatigue in the very high cycle regime.* Conference Proceedings. Institute of Meteorology and Physics, Vienna (2001).
23. Macha, E., Bedkowski, W. And Lagoda, T., *Multiaxial Fatigue and Fracture.* ESIS Publication 25, Elsevier (1999).
24. Suresh, S., *Fatigue of Materials*, 2nd edn. Cambridge University Press, Cambridge (1998).
25. Rice, C.R. (Ed.), *SAE Fatigue Design Handbook*, 3rd edn. AE-22, Society of Automotive Engineers, Warrendale (1997).
26. Hertzberg, R.W., *Deformation and Fracture Mechanics of Engineering Materials*, 4th edn. John Wiley & Sons, New York (1996).
27. Shiozawa, K. and Sakai, T. (Eds.), *Data Book on Fatigue Strength of Metallic Materials.* 3 Volumes. Elsevier, Amsterdam (1996).
28. *Fatigue and Fracture*. American Society for Materials, Handbook Vol. 19, ASM (1996).
29. *Fatigue Data Book: Light Structural Alloys.* ASM International (1995).
30. Dowling, N.E., *Mechanical Behavior of Materials. Engineering Methods for Deformation, Fracture, and Fatigue*, 3rd edn. Prentice-Hall (2006).
31. McDowell, D.L. and Rod, E. (Eds.), *Advances in Multiaxial Fatigue.* ASTM STP 1191 (1993).
32. Blom, A.F. and Beevers, C.J. (Eds.), *Theoretical Concepts and Numerical Analysis of Fatigue*. Proc. Conf. May 1992, Birmingham. EMAS (1992).
33. Klesnil, M. and Lukás, P., *Fatigue of Metallic Materials*, 2nd edn. Elsevier, Amsterdam (1992).
34. Brown, M.W. and Miller, K.J. (Eds), *Biaxial and Multiaxial Fatigue.* EGF Publication 3. Mechanical Engineering Publications (1989).
35. Boller, Chr. and Seeger, T., *Materials Data for Cyclic Loading.* Materials Science Monographs, 42, 5 Volumes. Elsevier, Amsterdam (1987).
36. Boyer, H.E., *Atlas of Fatigue Curves.* Amer. Soc. for Metals (1986).
37. Miller, K.J. and Brown, M.W. (Eds.), *Multiaxial fatigue*. ASTM STP 853 (1985).
38. Frost, N.E., Marsh, K.J. and Pook, L.P., *Metal Fatigue*. Clarendon, Oxford (1974).
39. Stephens, R.I., Fatemi, A., Stephens, R.R. and Fuchs, H.O., *Metal Fatigue in Engineering*, 2nd edn. John Willey & Sons (2000).